

CHEMICAL AND MINERALOGICAL CHARACTERISATION OF AGUADA  
PORTEZUELO POTTERY FROM CATAMARCA, NORTHWESTERN ARGENTINA.  
PIXE, XRD, AND SEM-EDS STUDIES APPLIED TO SURFACE PRE- AND  
POSTFIRING PAINTS, SLIPS, AND PASTES.

Authors

Guillermo A. De La Fuente\*, Víctor Galván Josa\*\*, Gustavo Castellano\*\*, Silvana  
Limandri\*\*, Sergio D. Vera\*, Johnny Ferraz Días\*\*\*, Sergio Suárez\*\*\*\*, Guillermo  
Bernardi\*\*\*\*, Silvana Bertolino\*\*

Institutional affiliations

\* Laboratorio de Petrología y Conservación Cerámica, Escuela de Arqueología, Universidad  
Nacional de Catamarca-CITCa., CONICET, Belgrano N° 300, (4700) Catamarca, Argentina.

Email: [gfuente2004@yahoo.com.ar](mailto:gfuente2004@yahoo.com.ar)

\*\*Instituto de Física Enrique Gaviola, CONICET-Universidad Nacional de Córdoba,

Argentina. Email: [galvan@famaf.unc.edu.ar](mailto:galvan@famaf.unc.edu.ar) / [gcas@famaf.unc.edu.ar](mailto:gcas@famaf.unc.edu.ar) /

[silvinalimandri@gmail.com](mailto:silvinalimandri@gmail.com) / [bertolin@famaf.unc.edu.ar](mailto:bertolin@famaf.unc.edu.ar)

\*\*\* Instituto de Física, Universidade Federal do Rio Grande do Sul, Brazil. [jfdias@if.ufrgs.br](mailto:jfdias@if.ufrgs.br)

This article has been accepted for publication and undergone full peer review but has not  
been through the copyediting, typesetting, pagination and proofreading process which may  
lead to differences between this version and the Version of Record. Please cite this article as  
doi: 10.1111/arcm.12517

\*\*\*Centro Atómico Bariloche, Comisión Nacional de Energía Atómica.

[bernardi@cab.cnea.gov.ar](mailto:bernardi@cab.cnea.gov.ar) / [suarez@cab.cnea.gov.ar](mailto:suarez@cab.cnea.gov.ar)

## Abstract

Particle induced X-ray emission (PIXE), X-ray diffraction (XRD), electron microprobe analysis (EDS), and scanning electron microscopy (SEM) analytical techniques have been used to characterize surface paints in pre- and post fired Aguada Portezuelo decorated pottery. Surface paintings in black, white, red, brown, burgundy, and other colours were analysed. Major, minor, and trace elements were detected by PIXE, whereas XRD and SEM-EDS gave information on the main mineral phases and the characteristic morphology for each analysed pigment. Results obtained indicate that the main colour groups can be easily discriminated by PIXE, and they are characterized by only one pigment for each colour, hematite (red) and Mn mineral oxides (black), respectively; whereas white pigments are characterized by calcite, ghelenite, and gypsum.

Keywords: PIXE, XRD, SEM-EDS, Aguada Portezuelo, Middle Period, Northwestern Argentina

## INTRODUCTION

Archaeological materials such as ceramics are examples of inhomogeneous systems at the micrometric scale. Their surface characteristics depend on their conservation state, which is related with the weathering suffered by the pieces. In general, the information related with their composition and manufacturing processes are not completely known. In this sense, chemical and crystallographic characterization techniques may provide valuable information. Nevertheless, the correct characterization of these materials is a challenge since standard destructive characterization procedures cannot be usually applied, due to the fact that keeping the material unaltered is a priority in cultural heritage samples.

From its beginning in the 70's, ion beam analysis (IBA) techniques have been successfully applied to study historical and cultural objects, and since the 90's they have been systematically used for material analysis (*e.g.* Ruvalcaba-Sil and Demortier 1997, Neelmeijer et al. 2000, Olsson et al. 2001, Ruvalcaba-Sil 2005, Hall 2006, Rizzuto et al. 2007, Rivero-Torres et al. 2008, Abd El Aal et al. 2009, Grassi et al. 2009, Popeou et al. 2010, Lima et al. 2011, Gajić-Kvašček et al. 2012, Rizzuto et al. 2014, Šmit et al. 2013, Calligaro et al. 2015, Pappalardo et al. 2015, 2016, Santos et al. 2015, Dasari et al. 2017). Nowadays, the advances in the characterization methodologies are centered in their application to areas with specific limitations, such as archaeometry. An excellent review of PIXE applications in archaeological ceramics is given by Rizzuto and Tabacniks (2017). Although the chemical state and crystallographic structure of compounds cannot be studied by IBA techniques, they allow the determination of elemental compositions with detection limits as low as a few ppm.

In addition, the thickness and composition of different layers forming the piece, as well as depth concentration profiles can be obtained by these techniques (Ruvalcaba-Sil et al. 1999). This information, along with mineralogical data provided by x-ray diffraction, allow archaeologists to address archaeometric questions regarding the provenance of the pieces, raw materials used, and the technology used in their production (De La Fuente et al. 2005, Bertolino et al. 2009, Galván Josa et al. 2010, Roumié et al. 2010, De La Fuente and Pérez Martínez 2008, 2018). Several limitations have to be taken into account for the proper interpretation of results, since many archaeological objects, particularly ceramic pieces, have been buried for over 1000 years, suffered weathering and partial removal of the paints, so the paint layer thickness is not homogeneous and the surfaces are rough (De La Fuente et al. 2005, Bertolino et al. 2009, Galván Josa et al. 2009, 2010).

This paper presents the analytical results obtained by combining PIXE, XRD and SEM-EDS techniques in the characterization of the archaeological paintings, slips and pastes of Aguada Portezuelo pottery belonging to Middle period of Catamarca valley (*ca.* 600-900 A.D.), Province of Catamarca, Northwestern Argentina. PIXE concentrations on major, minor, and trace elements for different color groups are further discussed. Chemical and mineralogical information is integrated to get a broad picture on the technological processes involved in the decoration of these vessels.

#### AGUADA PORTEZUELO CERAMIC STYLE

The Aguada Culture is one of the most spectacular of northwestern Argentina because of its iconographic complexity (also called the “draconian style”) and high technical skill apparent in the pottery. According to different studies, this culture emerged as a consequence of a

social and ideological change that occurred in the fourth to twelfth centuries of the Christian era in the Ambato Valley, and progressively spread out regionally to other geographical areas like Hualfín and Catamarca valleys, and northern La Rioja (González 1998, Baldini et al. 2002, Laguens 2005, Pantorrila and Regueiro 2006, Pérez Gollán 1991).

The Aguada Portezuelo ceramic style (*ca.* 600-900 A.D.), typical of the Catamarca valley, presents a great variation and complexity in the manufacturing techniques employed by the ancient potters, particularly the surface treatments and other decoration applied to the ceramic vessels (Kusch 1996-1997, González 1998, De La Fuente et al. 2005, Nazar and De La Fuente 2016, De La Fuente and Pérez Martínez 2008, 2018). Ceramic vessels have a complex technical elaboration process, involving at least two different firing steps during which several pigments were used by ancient potters as chromophores to obtain different coloured pre- and postfiring paintings (Nazar and De La Fuente 2016). One of the highlight characteristics of these ceramics is their marked polychromy, the motifs are complex use of negative and positive space, and the colors used range from purple red, reddish, black and yellow, this latter color unique in the archaeological ceramics from Northwestern Argentine (González 1998, Nazar and De La Fuente 2016: 167; Fig. 12, De La Fuente and Pérez Martínez 2008, 2018: 3; Fig. 1a). Sometimes, the colors have not been very well fixed by the firing and they appear as faint and dull, presenting pre- and postfiring paintings (Nazar and De La Fuente 2016: 166-172, De La Fuente and Pérez Martínez 2018: 6). Another of the technical decorative aspects rarely studied for this ceramic type is the use of resistant negative paintings (González 1998). Additionally, a manufacture attribute of particular importance is the surface treatment. The internal surface of the vessels is sometimes of an intense polished black color and in others it is burnished, perhaps involving a technical process of smoking the internal surface of the vessels, also so-called “*graffited*” (Nazar and

De La Fuente 2016: 168-171, De La Fuente and Pérez Martínez 2008, 2018:13). Extensive description and classification of Aguada Portezuelo ceramic style is given in Nazar and De La Fuente (2016) and De La Fuente and Pérez Martínez (2008, 2018).

Pre- and post-firing paintings of this pottery have been extensively analysed by Raman microspectroscopy, and in less intensively by XRD and SEM-EDS. Results of this previous research indicate that red and other colors are characterized exclusively by hematite pigment ( $\alpha\text{-Fe}_2\text{O}_3$ ), black colour presents a more variable composition, with Mn oxide minerals (pirolusite ( $\text{Mn}^{+4}\text{O}_2$ ) and psilomelane ( $\text{BaMn}^{+2}\text{Mn}_8\text{O}_{16}(\text{OH})_4$ ) ) predominantly responsible for this colour, and magnetite ( $\text{Fe}_3\text{O}_4$ )(sometimes titanomagnetite) are also present. White colour (a pre-firing slip) is the most variable compound, resulting from calcite ( $\text{CO}_3\text{Ca}$ ), gypsum ( $\text{CaSO}_4 \cdot 2\text{H}_2\text{O}$ ), and gehlenite ( $\text{Ca}_2[\text{Al}_2(\text{SiO}_2)]$ ) mineral phases, although titanium oxide ( $\text{TiO}_2$ ) and hydroxyapatite ( $\text{Ca}_{10}[\text{PO}_4]_6[\text{OH}]_2$ ) have also been identified (Cremonte et al. 2003, De La Fuente et al. 2005, Bertolino et al. 2009, Galván Josa et al. 2009, 2010, De La Fuente and Pérez Martínez 2008, 2018).

## SAMPLING

Pottery sherd samples were chosen from a collection for being representative or unique in their technological classes. Different samples were considered, all corresponding to the Aguada Portezuelo ceramic style, as described above. They were collected at four different sites: Tiro Federal Sur, Portezuelo, La Viñita and R. Recalde, all within the Catamarca valley (Fig. 1a). Sample selection for further analyses followed pigment conservation criteria.

A set of 19 pottery sherds were studied (Table 1 and 2). Figure 1b displays some pictures of the samples analyzed, in which the colors characterized were white, black, reddish, dark brown, light brown, purple red or burgundy and ocher. In order to ensure the PIXE results correspond only to the paint thickness, some of these samples were chosen for the characterization of the paste: M49, M7, M15, MX3 (fine texture) and M9 (coarse texture). All these pieces bear approximate dimensions  $1.5\text{cm} \times 1\text{cm}$ , excepting sample M16 ( $4\text{cm} \times 4\text{cm}$ ). Table 1 gives information about the main characteristics of the sherds.

## ANALYTICAL TECHNIQUES

Chemical and mineralogical characterizations were carried out using PIXE, SEM-EDS and XRD. The experimental conditions are detailed below, as well as the methodology followed for sample preparation and data processing in each case.

### *PIXE*

Pottery sherds were analyzed using a 2 MeV proton beam in two different tandem accelerators: a NEC 1.7 MV accelerator from Centro Atómico Bariloche (CAB, Argentina) and a NEC 3 MV accelerator from the Universidad Federal de Rio Grande do Sul (UFRGS, Brazil). The first one has a high-counting rate SDD x-ray detector with an ultrathin polymer window, allowing the detection of energies ranging from 0.2 to 20 keV. The second one has a Si (Li) conventional detector with a Be window, bearing a better efficiency for high energy lines, i.e., from 1 to 26 keV. In order to minimize radiation damage effects, low beam

currents were used, around 0.5 nA. In all cases, the beam spot area at the sample surface was 1 to 9 mm<sup>2</sup>.

PIXE spectra were processed with the GUPIX software (GUPIXWIN v.2.2.4 Copyright (C) 2005. University of Guelph). For the spectra acquired at CAB, the analyses were performed as elemental quantifications, including O and C. For the spectra measured at UFRGS, oxygen characterization was carried out by stoichiometric association to the visible elements, through the most stable oxides; in these cases, it was not possible to quantify the carbon content. A statistical package developed at MURR was used for the interpretation of the data. Statistical analysis was carried out on base-10 logarithms of the concentrations of all 25 chemical elements. The methods used to interpret compositional data obtained from the analysis of archaeological materials are discussed in detail elsewhere (e.g. Bishop and Neff 1989; Glascock 1992; Neff 2000, 2002) and will not be described in detail here. Cluster and principal component analyses were performed for the PIXE data set. Groups were initially defined on the basis of visual separation and further refined using group membership probabilities based on Mahalanobis distance projections (Bishop and Neff 1989).

### *XRD*

X-ray diffraction was used to characterize paints in pieces for which a reasonable amount of sample could be scraped from the surface. XRD patterns were recorded with a Philips X'Pert PRO PW3040/60 diffractometer, with Cu K $\alpha$  X-ray radiation, Si monochromator, at 40 kV and 30 mA, step scan at 0.3°/min and step size of 0.02° 2 $\theta$ . In all cases, only a small amount (a few milligrams) of material was available, so samples were mounted on a Si holder of low background.



## *SEM-EDS*

Scanning electron microscopy and microanalysis was carried out in a JEOL JXA 8230 equipment at Laboratorio de Microscopía de Rayos X (LAMARX), at National University of Córdoba, Argentina. Measurements were done with a electron 15 keV electron beam, and a current of 9 nA. Samples were covered with Au in order to avoid charge accumulation effect.

## RESULTS AND DISCUSSION

### *PIXE*

Figure 2 displays an example of the x-ray emission spectra obtained with each of the experimental setups described above. As can be seen, these examples show the advantages and disadvantages of each detection system. The detector attached to the NEC 1.7 MV (ultrathin polymer window) allows to detect light elements as C and O, although its efficiency rapidly decays for energies greater than 10 keV, which hinders the appropriate detection of elements such as Rb and Sr –although L emission could be registered, the detector resolution inhibits the adequate deconvolution from K-lines emitted by other major components (Si). On the other hand, the detector attached to the NEC 3 MV (beryllium window) is not well suited for the detection of elements with atomic number below 10, but it exhibits a high efficiency for detecting characteristic energies above 10 keV.

Table 2 displays the quantification results after processing the spectra. In the reddish paints, different tones are present, which might be correlated with hematite ( $\alpha\text{Fe}_2\text{O}_3$ ) content

(Bertolino et al. 2009, Galvan Josa et al. 2010). This is observed in the Fe concentration with an average of 18,5% in samples M38, MX and M7 (range of 17,3-20,2%), whereas the more intense burgundy samples M2, M15 and M18 have a higher Fe content of around 23,8% in average, and a range of 13,42-30,44%. Brown paint samples such as M28 also have a high Fe content (31,88%), but, unlike the reddish paints, a higher Mn concentration is present (8,33%). Light brown regions (M31) were painted over a white base, and present lower concentrations for Fe (14,51%) and Mn (3,04%) than sample M28. A careful examination of the colored region of this sample showed a deteriorated and non-homogeneous spoiled surface; thus, the beam could have also reached the substrate of the colored region (paste), which is reflected in the higher Al (8,37%) and Si (15,47%) contents. Regarding the other paints, the composition obtained was very dissimilar, with variable Fe content ranging from 3,62% (M24) to 8,21% (M16). Also, it is observed great differences in transition metals like Cr, Cu, and Zn. The composition of this paint is similar to that of the paste (mainly high concentration of Si associated to glass and quartz), though richer in Ca.

Concerning the trace elements, it is important to observe that Ba was detected in four out of five black postfiring paintings analyzed. Additionally, it seems that the amount of barium is positively correlated with the Mn concentration. This suggests that the black colour precursor might be psilomelane mineral group ( $\text{BaMn}^{2+}(\text{Mn}^{4+})_8\text{O}_{16}(\text{OH})_4$ ), a hydrous manganese oxide with variable amounts of barium and potassium. Psilomelane group includes hollandite and romanachite minerals. Psilomelane sometimes is present with vanadinite intergrowth crystals, which perhaps could explain the V/Ba positive correlation observed in the PIXE results.

Vanadinite also occurs associated with barite, a barium sulfate ( $\text{BaSO}_4$ ), although the lack of Pb in these samples makes difficult to explain this correlation. In previous analytical research done on Aguada Portezuelo paints it was determined that the main identified mineral for this

colour was pyrolusite ( $\text{MnO}_2$ ), since Ba lines were not detected by EDS (De La Fuente et al. 2005).

Results obtained by PCA for major, minor, and trace elements indicate that black, white, and reddish-burgundy paintings might be divided in three groups, according to the Fe/Mn ratio, Ca content, and the different Fe concentrations, respectively (Fig. 3a, and 3b). Figure 3a displays the PC1 and PC2 plot with the elements projections and the three groups defined by Mahalanobis distance; whereas Fig. 3b shows the loading for the elements influencing each of the component. The first 4 PC's explain 73,4% of the variance. Table 3 gives the chemical information for each defined group.

Group 1, the black paintings, presents variable concentrations of Fe and Mn, and in some cases they positively correlate (Fig. 3a). They can be divided in three subgroups according to the Fe/Mn ratio: subgroup A, Fe/Mn: 0,515 (M18, M24) with 19,12% Mn and 9,09% Fe average, subgroup B, Fe/Mn: 0,47 (M50, M28) with 10,52% Mn and 20,85% Fe average, and subgroup C, Fe/Mn: 0,32 (M1) with 27,69% Mn and 8,96% Fe (Fig. 3c, Table 2). One sample, M15 is definitely an outlier, with a Fe/Mn: 1,78 (16,35% Mn and 29,14% Fe). This variation in the ratio of Fe/Mn is also expressed in Raman analysis with the alternative presence of Mn oxide minerals and hematite compounds (De La Fuente and Pérez Martínez 2008, 2018).

Group 2 shows the white paintings. Here, three subgroups were found: subgroup A (M57, M28) with an average of 25,22% Ca; subgroup B (M47, M45, M24, M16) with an average of 27,22% Ca, and subgroup C (M52) with a Ca concentration of 15,78% (Fig. 3c). Sample M13 is an outlier with 14,12% Ca concentration. Some white paintings (subgroup B) exhibit different Pb (lead) in trace concentrations (ppt). In translucent media, like quartz, Pb might be

the precursor of white colour (Bertolino et al. 2009, Galvan Josa et al. 2010). Also, the presence of Pb in low concentrations in prefiring paintings sometimes is indicative of the use as a fluxing agent to achieve an initial glazed-type ceramics (Van Keuren et al. 2013, Ferguson et al. 2017). Additionally, it is interesting to observe that one sample, M52, has an unusual amount of P (6852 ppm), which could be indicative of hydroxyapatite presence (Table 2) (see Cremonte et al. 2003).

On the other hand, PCA also clearly differentiates another group (Group 3) involving mostly reddish and burgundy colour samples (Fig. 3a). As contrarily thought, samples are discriminated in this group more as a function of the relative concentrations of transition metals (Cr, Ni, Cu, Zn) than following the Fe concentrations: subgroup A, samples M7 and M15 with an average of 23,84% Fe; subgroup B, samples M38 and M18 with an average of 23,93% Fe; and subgroup C, sample M2 with 13,42% Fe. A subgroup D, after projected samples for membership probabilities, is formed by samples MX, MX3 (paste), M7 (paste), and M9 (paste) with 7,64% Fe. One other sample, M16, is also plotted in the margin of this group (Fig. 3c). Burgundy samples also present an unusual amount of Cu, Ni and Zn (ppm) in all the samples analysed, whereas other samples show higher Ca concentrations (Table 2). Therefore, it can be observed that different tonalities do not match with exact different chemical compositions, mainly of Fe concentration. The presence of Fe as different iron oxides (like hematite) gives the red colour for these paintings (mostly postfiring), although the chemical variations observed are due mainly to the presence of different concentrations of trace elements like Cu, Zn, Ba, and Zr. Different tonalities in postfiring paintings are due to different recipes used by ancient potters involving different mixed minerals as colorants. The subgroups observed for the red iron based paintings are related with the origin of raw materials used by potters.

A further exploration using only minor and trace elements was carried out by cluster analysis (Fig. 3d). Results show higher variations between samples of the same colour (e.g. white and black), although for burgundy/reddish/ocher/brown samples the plot shows a good discrimination based on the Euclidean distances. Trace elements responsible for this discrimination are Cr, Cu, Zn, and Zr. These preliminary results could indicate that several geochemically different sources of raw materials were introduced to produce these red iron based pigments, mainly reddish, burgundy, brown, and ocher.

### *XRD*

XRD was applied to white pre-firing slips, and ocher and reddish post-firing paints (Fig. 4a). Also, some paste analyses were carried out. In all cases, the extracted materials also contained some grains from the underlying pastes, which is reflected in the bulk mineralogy by presence of quartz, feldspars, micas, amphibole, and hematite. As shown in Fig. 4a, white paints are characterized by Ca-bearing minerals like ghelenite, calcite, and gypsum (cf. De La Fuente and Pérez Martínez 2008, 2018). In some cases, both the low intensity of reflections of micas and feldspars, and the presence of new higher temperature mineral phases (hematite and ghelenite) were observed. Ghelenite is an aluminosilicate that forms from mixtures of calcite with clay minerals (paste) at temperatures between 850 °C - 900 °C and 1050°C, and beyond that temperature it forms anorthite. This indicates that the firing temperature may have reached or exceeded 900 °C – 1000 °C, as previously reported by Bertolino et al. (2009). Ghelenite and CaO in ceramic pastes could be an indication of the presence of calcite in the original raw material, and it could act as a flux to decrease the required firing temperature, also contributing to the vitrification and the formation of vesicles to liberate CO<sub>2</sub>. As

pointed out by Bertolino et al. (2009: 97, Fig. 4) if dissociation of calcite was not completed (~ 750 °C – 850°C), the sequence of gehelenite, calcite, and CaO may coexist in the range of 700 °C – 900 °C. The absence of gehelenite might be an indication of lower firing temperatures around 900 °C (Bertolino et al. 2009:98). Gypsum has been reported at least by three researchers as used as a decorative white pigment (Palamarczuk et al. 2007, Centeno et al. 2012, Freire et al. 2018). The presence of gypsum as prefiring white paint in one sample (M16) is difficult to explain (Fig. 1 and Fig. 4a). This sample has the highest Ca (42.3 wt%) and S (4309 ppm) concentrations among the white samples (Table 2). Gypsum is a calcium sulfate dehydrate mineral ( $\text{CaSO}_4 \cdot 2\text{H}_2\text{O}$ ) and, it is both, available in nature from chemical sedimentary rock formations, or generally culturally produced through a calcining technology using limestone rocks (*aljez*) (Harrell 2014, 2017). The impure form of gypsum is called gypsite, and it is present in some natural soil formations. Bassanite ( $\text{CaSO}_4 \cdot 1/2\text{H}_2\text{O}$ , calcium sulfate hemihydrate) and anhydrite ( $\text{CaSO}_4$ , anhydrous calcium sulfate) are other forms of calcium sulfates, and they are subsequently obtained by dehydration of original gypsum through heating (Harrell 2017:537). The presence of gypsum as a slip in the vessels (perhaps mixed with clay) implies that its application on the ceramic surface by potters was in a postfiring context, since its physical and chemical properties change through subsequent higher temperatures giving different forms of anhydrite –or “dead gypsum”–(Villanueva Dominguéz and García Santos 2001). It is not clear yet if the gypsum was obtained by heating the *aljez* or from gypsite deposits, although the evidence of use of gypsum in rock art in the area, and the discovering of a natural gypsum source points out to the use of this source in prehispanic times (De La Fuente and Nazar 2016). Finally, ocher and reddish postfiring paintings analysed in this work are characterized by hematite (Fig. 4a) (De La Fuente and Pérez Martínez 2008, 2018, Bertolino et al. 2009).

### *SEM –EDS*

The paste analysis by SEM allows the observation and identification of materials almost completely melted, characterized by vitreous textures with an important bubble and tubule abundance created by escaping gases during the paste melting process (Fig. 4b). Within pores, very fine grained materials can be distinguished, composed of Ca, Fe or Si (Fig. 4c). These can be interpreted as new phases produced by the reaction of mineral components at high temperatures (Bertolino et al. 2009, Galvan Josa et al. 2010).

Irregular and very fine particle aggregates, eventually less than 200nm in the vesicule walls or forming part of the matrix, have been observed (Fig. 4c). They have a highly variable composition, but always bearing high O concentration (probably oxides), contrasting with the paste compositions. EDS analyses on white, black and ocher paintings show very similar results to those obtained by PIXE (Fig. 4d; Table 2). In all the samples, white paint has high Ca content, the black one, Fe and Mn plus minor Ca (Fig. 4d). Ocher paint shows medium to high Fe concentrations, and also Ca from the substratum. All the paints do have an aluminosilicate composition (Al + Si) evidencing the existence of a clayish vehicle to transport the colourant pigment (Fig. 4d) in accordance with previous SEM-EDS research done on this pottery (De La Fuente et al. 2005, also see De La Fuente and Pérez Martínez 2008: 181, Fig. 10). It is unknown if a flux or binder has been added to the Al + Si + pigment system, before (for the white slip) and/or after (for reddish, burgundy, ocher, and black paintings) the firing, although the examination of hundreds of sherds of Aguada Portezuelo pottery shows for the postfiring colours an unusual amount of pigment applied on the surface of the vessels

suggesting the possibility of some kind of binder applied to fix the pigment into the porous ceramic surface.

## CONCLUSIONS

Multielemental PIXE chemical results, in combination with a robust PCA statistical treatment of data allowed the examination of the compositional ranges of various pre- and postfiring paintings on Aguada Portezuelo pottery. Nowadays, the main advantage of PIXE is its almost non destructive nature, and the possibility to obtain concentrations of ppm and even ppt for certain specific elements. In the present study, different painting colour groups (black, white, and burgundy/reddish) could be rapidly discriminated by PIXE. Particularly in black paintings, the presence of different Fe/Mn ratios with the presence of barium suggests the use of psilomelane group mineral as an inorganic mineral precursor for the postfiring black paintings. Manganese oxide based minerals are often chemically complex. Psilomelane group involves at least two oxides, hollandite and romanchite, and it has an amorphous nature containing admixed impurities such as iron hydroxides. Thus, it is easily processed by potters as a pigment. White prefiring slips are chemically characterized by calcium expressed in different concentrations, although through XRD different Ca-bearing metastable mineral phases like calcite, gehlenite, and gypsum were identified. Interestingly, one white sample determined by PIXE showed an unusual P concentration, suggesting the possibility of hydroxyapatite presence in the prefiring slip. Burgundy, reddish, and ocher postfiring paintings are clearly characterized by iron (Fe), where  $\alpha$  hematite was the main pigment used by ancient potters. Trace element analysis did not produce direct correlations between paint



Accepted Article

color and chemical compositions, probably mainly due to the different recipes applied by potters. However, trace elements discriminated fairly well these tonalities suggesting the use of different geochemical sources of raw materials for the pigments. Definitely, PIXE studies have much to do in the future in the identification of different iron oxides pigment sources used by ancient potters, especially by using minor and trace elements (see David et al. 1991, Erlandson et al. 1999, Lebon et al. 2018). Comparatively with vibrational techniques like Raman microspectroscopy, PIXE allows to explore the compositional chemical concentrations of the main pigments involved in the decoration of the vessels, thus complementing the information achieved through other analytical techniques. Finally, SEM-EDS studies contributed to a better understanding of the changes overcome, through different firing temperatures, in the physical and chemical structure of the ceramic matrixes.

## ACKNOWLEDGMENTS

This research was fully funded by National Research Scientific Council (CONICET), Argentina. V. G. and S. L. acknowledge CONICET for partial funding through different postdoctoral fellowships to develop the PIXE analyses. The Direction of Anthropology, Government of Province of Catamarca, provided permission to analyze the samples under the project “Cadenas Operativas y Elecciones Tecnológicas en la Producción de Alfarería Arqueológica y Pinturas Rupestres durante el Período Agroalfarero Medio (ca. AD 600 – AD 900) en la Cuenca Ipizca-Icaño (Dptos. Ancasti y La Paz, Catamarca, Argentina): Una Aproximación Arqueométrica”.

## REFERENCES

- Abd El Aal, S., Korman, A., Stonert, A., Munnik, F., Turos, A., 2009, Ion beam analysis of ancient Egyptian wall paintings. *Vacuum* 83, S4-S8.
- Baldini, M., Carbonari, J., Cieza, G., de Feo, M., del Castillo, M., Figini, A., Rex González, A., Huarte, R., Togo, J., 2002, Primer análisis de la cronología obtenida en el sitio Choya 68 (Depto. de Capayán, Provincia de Catamarca, Argentina). *Estudios Atacameños* 24, 71-82.
- Bertolino, S.R., Galván, V., Carreras, A., Laguens, A., De La Fuente, G., Riveros, A., 2009. X-ray techniques applied to surface paintings of ceramic pottery pieces from Aguada Culture (Catamarca, Argentina). *X-Ray Spectrometry* 38, 95-102.
- Bishop, R. L., and Neff, H., 1989, Compositional data analysis in archaeology, in *Archaeological Chemistry I. Advances in Chemistry, Series 220* (ed. R. O. Allen), 57-86. American Chemical Society, Washington, D. C.
- Calligaro, T., González, V., Pichon, L., 2015, PIXE analysis of historical paintings: Is the gain worth the risk?. *Nuclear Instruments and Methods in Physics Research B* 363, 135-143.



- Centeno, S., Williams V., Little N., Speakman J., 2012 Characterization of surface decorations in Prehispanic archaeological ceramics by Raman spectroscopy, FTIR, XRD and XRF. *Vibrational Spectroscopy* 58: 119-124.
- Cremonese, M. B., Baldini, M., Botto, I. L., 2003, Pastas y colores. Un camino al conocimiento del estilo Portezuelo de Aguada. *Intersecciones en Antropología* 4, 3-16.
- Dasari, K. B., Acharya, R., Ray, D. K., Lakshmana Das, N., 2017, Application of PIXE for the determination of transition elements in the grouping study of archaeological clay potteries. *X-Ray Spectrometry* 46, 180-185.
- David, B., Clayton, E., Watchman, A., 1993, Initial results of PIXE analysis on northwestern Australian ochers. *Australian Archaeology* 36, 50-57.
- De La Fuente, G. A., Kristcautzky, N., Toselli, G. A., Riveros, A., 2005, Petrología cerámica comparativa y análisis composicional de las pinturas por MEB-EDS de estilo Aguada Portezuelo (ca. 600-900 DC) en el valle de Catamarca (Noroeste Argentino). *Estudios Atacameños* 30: 61-78.
- De La Fuente, G. A., Pérez Martínez, J. M., 2008, Estudiando pinturas en cerámicas arqueológicas “Aguada Portezuelo” (ca. 600-900 AD) del Noroeste Argentino: nuevos aportes a través de una aproximación arqueométrica por microespectroscopía de Ramán (MSR). *Intersecciones en Antropología* 9, 173-186.

De La Fuente, G. A., Pérez Martínez, J. M., 2018, Ancient potters, paintings and craft specialization in northwestern argentine region: new data through Raman characterization of pre- and postfiring ceramic paintings on Aguada Portezuelo Ceramics from Middle Period (Catamarca, Argentina). *Archaeological and Anthropological Sciences*, DOI 10.1007/s12520-018-0676-9

Erlandson, J. M., J. D. Robertson, Descantes C., 1999, Geochemical analysis of eight red ochres from western North America. *American Antiquity* 64, 517-526.

Ferguson, J. R., S. Van Keuren, Bender S., 2015, Rapid qualitative compositional analysis of ceramic paints. *Journal of Archaeological Science: Reports* 3, 321-327.

Freire, E., Halac, E. B., Polla, G., Reinoso, M., Basile, M., Ratto, N., 2018, Análisis de rellenos en surcos incisos y excisos en pucos de Fiambalá (Catamarca, Argentina), *Intersecciones en Antropología* 19: 17-24.

Gajić-Kvašček, M., Stojanović, M. M., Šmit, Ž., Kantarelou, V., Karydas, A. G., Šljivar, D., Milovanović, D., Andrić, V., 2012, New evidence for the use of cinnabar as colouring pigment in the Vinča culture. *Journal of Archaeological Science* 39, 1025-1033.

Galván Josa, V., Bertolino, S., A., Riveros, J., Castellano, G., 2009, Methodology for processing backscattered electron images. Application to Aguada archaeological paints. *Micron* 40: 793-799.

Galván Josa, V., Bertolino, S., Laguens, A., Riveros, J., Castellano, G., 2010, X-ray and Scanning Electron Microscopy archaeometric studies of pigments from the Aguada Culture, Argentina. *Microchemical Journal* 96, 259-268.

Glascock, M. D., 1992, Characterization of archaeological ceramics at MURR by neutron activation analysis and multivariate statistics, in *Chemical Characterization of Ceramic Pastes in Archaeology* (ed. H. Neff), 11-26, Prehistory Press, Madison, WI.

González, A. 1998, *Arte Precolombino. Cultura La Aguada. Arqueología y sus diseños*. Filme Ediciones Valero.

Grassi, N., Bonanni, P., Mazzotta, C., Migliori, A., Mandò, P. A., 2009, PIXE analysis of a painting by Giorgio Vasari. *X-Ray Spectrometry* 38, 301-307.

Hall, B., 2006, *PIXE analysis of oil-paint pigments: proof of principle*. Bachelor of Science Thesis. Department of Physics and Astronomy, Brigham Young University.

Harrell, J. A., 2014, Report of geological prospection in the vicinity of Amarna. *Journal of Egyptian Archaeology* 100, 25-33.

Harrell, J. A., 2017, Amarna gypsite: A new source of gypsum for ancient Egypt. *Journal of Archaeological Science: Reports* 11, 536-545.

Ikeoka, R.A., Appoloni, C.R., Rizzutto, M.A., Silva T.F., Bandeira, A.M., 2013, PIXE analysis of pre-colonial pottery from Sambaqui do Panaquatira, *13th PIXE conference*,

Kusch, M.F. 1996-97, Estructura y diseño en la cerámica Portezuelo. *Shincal* 6: 241-248.

Lebon, M., L. Pichon, Beck, L., 2018, Enhanced identification of trace element fingerprint of prehistoric pigments by PIXE mapping. *Nuclear Instrumentation and Methods in Physics Research B* 417, 91-95.

Lima, S.C., Rizzutto, M.A., Added, N., Barbosa, M. D. L., Trindade, G. F., Fleming, M. I. D. A., 2011, Pre-Hispanic ceramics analyzed using PIXE and radiographic techniques. *Nuclear Instruments and Methods in Physics Research B* 269, 3025-3031.

Nazar, D. C., De La Fuente, G. A., 2016, Acerca de la cerámica Aguada Portezuelo del Valle de Catamarca y la Sierra de Ancasti. *Comechingonia* 20, 153-188.

Neelmeijer, C., Brissaud, I., Calligaro, T., Demortier, G., Hautojärvi, A., Mäder, M., Martinot, L., Schreiner, M., Tuurnala, T., Weber, G., 2000, Paintings –a Challenge for XRF and PIXE analysis. *X-Ray Spectrometry* 29, 101-110.

Neff, H., 2000, Neutron activation analysis for provenance determination in archaeology, in *Modern Analytical Methods in Art and Archaeology* (eds. E. Ciliberto and G. Spoto), 81–134. John Wiley and Sons, Inc., New York.

Neff, H., 2002, Quantitative techniques for analyzing ceramic compositional data, in *Ceramic Source Determination in the Greater Southwest* (eds. D. M. Glowacki and H. Neff), , Monograph 44, Cotsen Institute of Archaeology, UCLA, Los Angeles

Olsson, A. –M. B., Calligaro, T., Colinart, S., Dran, J. C., Lövestam, N. E. G., Moignard, B., Salomon, J., 2001, Micro-PIXE analysis of an ancient Egyptian papyrus: identification of pigments used for the “Book of the Dead”. *Nuclear Instruments and Methods in Physics Research B* 181, 707-714.

Palamarczuk, V., M. E. Fernández de Rapp, G. E. Lascalea, 2007, Aproximaciones a la caracterización del material blanco decorativo de la cerámica Famabalasto Negro Grabado, in *Cerámicas Arqueológicas. Perspectivas Arqueométricas para su Análisis e Interpretación* (eds. M. B. Cremonte and N. Ratto), pp. 27-37. Editorial de la Universidad Nacional de Jujuy, Jujuy, Argentina.

Pantorrilla, M., Núñez Regueiro, V., 2006. Investigaciones arqueológicas en la zona de Escaba, provincia de Tucumán: asentamientos Condorhuasi y Aguada en las Yungas. *Intersecciones en Antropología* 7, 235-245.

Pappalardo, L., La Rosa, V., Rizzo F., Romano, F. P., 2015, Non-destructive PIXE –alpha characterisation of pigments in Kamares pottery (1850-1700 BC) from Phaistos (Crete). *X-Ray Spectrometry* 44, 276-281.



Pappalardo, L., Barresi, S., Biondi, G., Caliri, C., Caruso, F., Catalano, R., Lamagna, G., Manenti, G. A., Monterosso, G., Orlando, A., Rizzo, F., Romano, F. P., Santos, H. C., 2016, PIXE –alpha non-destructive and *in situ* compositional investigation of black gloss on ancient pottery. *X-Ray Spectrometry* 45, 258-262.

Pérez Gollán, J., 1991. La Cultura de la Aguada vista desde el Valle de Ambato.

*Publicaciones Arqueología CIFFyH*, Córdoba. 46, 157-174.

Poupeau, G., Le Bourdonnec, F.-X., Carter, T., Delerue, S., Shackley, M. S., Barrat, J.-A.,

Dubernet, S., Moretto, P., Calligaro, T., Milić, M., Kobayashi, K., 2010, The use of SEM-EDS, PIXE and EDXRF for obsidian provenance studies in the Near East: a case study from Neolithic Çatalhöyük (central Anatolia). *Journal of Archaeological Science* 37, 2705-2720.

Rivero-Torres, S., Calligaro, T., Tenorio, D., Jiménez-Reyes, M., 2008, Characterization of archaeological obsidians from Lagartero, Chiapas Mexico by PIXE. *Journal of Archaeological Science* 35, 3168-3171.

Rizzuto, A. M., Tabacniks, M. H., 2017, Particle Induced X-ray Emission (PIXE) and its application in ceramic analysis, in *The Oxford Handbook of Archaeological Ceramic Analysis* (ed. A. Hunt), pp. 23-54. Oxford Handbooks Online, Oxford, UK.

Rizzuto, A. M., Tabacniks, M. H., Added, N., Barbosa, M. D. L., Curado, J. F., Pascholatt, P. R., Neves, G., Lima, S. C., and Melo, H. G., 2007, Pixe Externo para Análises de

Objetos de Arte e Arqueologia, *Revista Brasileira de Arqueometria, Restauração e Conservação* 1, 309-312.

Rizzutto, M.A., Moro, M.V., Silva, T.F., Trindade, G.F., Added, N., Tabacniks, M.H., Kajiya, E.M., Campos, P.H.V., Magalhães, A.G., Barbosa, M., 2014, External-PIXE analysis for the study of pigments from a painting from the Museum of Contemporary Art. *Nuclear Instruments and Methods in Physics Research B* 332, 411-414.

Roumié, M., U. Wicenciak, E. Bakraji, B. Nsouli, 2010. PIXE characterization of Lebanese excavated amphorae from Jiyeh archeological site. *Nuclear Instruments and Methods in Physics Research Section B: Beam Interactions with Materials and Atoms* 268, 87-91.

Ruvalcaba-Sil, J. L., 2005, PIXE Analysis of Pre-Hispanic Items from Ancient America, in *X-rays for Archaeology*, Uda, M., Demortier, G., Nakai, I. (eds), pp. 123-149. Springer, Dordrecht.

Ruvalcaba-Sil, J. L., Demortier, G., 1997, Scanning RBS-PIXE study of ancient artifacts from South America using microbeam. *Nuclear Instruments and Methods in Physics Research B* 130, 297-302.

Ruvalcaba-Sil, J.L., M.A. Ontalba Salamanca, L. Manzanilla, J. Miranda, J. Cañetas Ortega, C. López, 1999, Characterization of pre-Hispanic pottery from Teotihuacan, Mexico, by a combined PIXE-RBS and XRD analysis. *Nuclear Instruments and Methods in Physics Research B* 150, 591-596.

Santos, H.C., Added, N., Silva, T.F., Rodrigues, C.L., 2015, External-RBS, PIXE and NRA analysis for ancient swords. *Nuclear Instruments and Methods in Physics Research B*, 345, 42-47.

Šmit, Ž., Milavec, T., Fajfar, H., Rehren, Th., Lankton, J.W., Gratuze, B., 2013, Analysis of glass from the post-Roman settlement Tonovcov grad (Slovenia) by PIXE–PIGE and LA-ICP-MS. *Nuclear Instruments and Methods in Physics Research B* 311, 53-59.

Van Keuren, S., H. Neff, Agostini, M. R., 2013, Glaze-paints, technological knowledge and ceramic specialization in the fourteenth-century Pueblo Southwest. *Journal of Anthropological Archaeology* 32, 675-690.

Villanueva Dominguéz, L., García Santos, A., 2001, *Manual del Yeso*. Asociación Técnica y Empresarial del Yeso. S. L. CIE Inversiones Editoriales Dossat. Madrid.

Acc

Table 1. Main characteristics of the Aguada Portezuelo sherds

Sample Number	Site	Ceramic Form	Vessel Form	Internal colour	External colour	Core colour	Texture	Firing	Surface treatment	Decoration
M1	TSF	globular	lip/neck	4/N black	2.5YR 5/6 red - 10YR 3/1 black - 2.5Y 8/2 white	6/N gray	fine	reduced	smoothed-polished internal /external surface	postfiring painting external surface
M2	TFS	bowl	body	4/N black	2.5Y 5/6 red - 7.5YR 6/6 brownish	6/N gray	fine	oxidized	smoothed-polished internal /external surface	prefiring painting external surface <i>graffited</i> internal surface
M7	TFS	globular vessel	body	4/N black	2.5Y 8/1 white - 2.5YR 5/6 red	6/N gray	fine	reduced	smoothed-polished internal /external surface	postfiring painting external surface polished - <i>graffited</i> internal surface
M9	TFS	globular vessel	body	7.5YR 5/4 brownish	2.5Y 8/1 white	7.5YR 5/4 brownish	coarse	oxidized	smoothed internal /external surface	postfiring painting external surface
M13	Port	vessel	body	3/N black	2.5Y 3/1 black - 10R 4/3 red - 7.5YR 5/4 brownish - 2.5Y 8/1 white	4/N black	fine	reduced	smoothed-polished internal /external surface	pre- and postfiring painting internal / external surface
M15	Port	vessel	body	2.5Y 3/1 black - 7.5YR 5/4 brownish	7.5YR 5/4 brownish - 10R 4/3red	7.5YR 5/4 brownish	fine	oxidized	smoothed-polished internal /external surface	pre- and postfiring painting internal / external surface
M16	Port	globular vessel	body	4/N black	2.5Y 3/1 black - 2.5Y 8/1 white -	6/N gray	fine	reduced	smoothed-	postfiring painting

					7.5YR 6/6 yellow				polished internal /external surface	external surface / graffited internal surface
M18	Port	globular vessel	body	4/N black	10R 4/3 red - 2.5YR 3/1 black - 2.5Y 8/1 white	6/N gray	fine	reduced	smoothed-polished internal /external surface	postfiring painting external surface <i>graffited</i> internal
M24	TFS	globular vessel	body	4/N black	2.5Y 8/1 white - 7.5YR5/4 brownish - 2.5Y 3/1 black	6/N gray	fine	reduced	smoothed-polished internal /external surface	postfiring painting external surface <i>graffited</i> internal
M28	LV	vessel	body	4/N black	2.5Y 3/1 black - 2.5Y 8/1 white - 7.5YR 5/4 brownish	6/N gray	fine	reduced	smoothed-polished internal /external surface	postfiring painting external surface <i>graffited</i> internal surface
M31	RR	globular vessel	body	4/N black	7.5 YR 5/4 brownish - 2.5Y 8/1 white	6/N gray	fine	reduced	smoothed-polished internal /external surface	postfiring painting external surface <i>graffited</i> internal surface
M37	TFS	globular vessel	body	7.5YR 5/4 brownish	2.5YR 5/6 red - 7.5YR 5/4 brownish	7.5YR 5/4 brownish	fine	oxidized	smoothed-polished internal /external surface	prefiring painting external / internal surface
M45	Port	globular vessel	body	4/N black	2.5Y 3/1 black - 2.5Y 8/1 white	5/N gray	fine	reduced	smoothed-polished internal /external surface	postfiring painting external surface <i>graffited</i> internal surface
M47	Port	globular vessel	body	4/N black	2.5Y 8/1 white	6/N gray	fine	reduced	smoothed-polished internal /external surface	postfiring painting external surface <i>graffited</i> internal surface

M49	Port	globular vessel	body	7.5YR 5/4 brownish	7.5YR 5/4 brownish	7.5YR 5/4 brownish	fine	oxidized	smoothed internal /external surface	prefiring painting external / internal surface
M50	Port	bowl	body	4/N black	2.5Y 3/1 black - 7.5YR 5/4 brownish	6/N gray	fine	reduced	smoothed-polished internal /external surface	postfiring painting external surface <i>graffited</i> internal surface
M52	Port	vessel	body	4/N black	2.5Y 8/1 white	6/N gray	fine	reduced	smoothed-polished internal /external surface	postfiring painting external surface <i>graffited</i> internal surface
M57	Port	globular vessel	body	4/N black	2.5Y 8/1 white	6/N gray	fine	reduced	smoothed-polished internal /external surface	postfiring painting external surface <i>graffited</i> internal surface
MX	Port	globular vessel	body	4/N black	10R 4/3 red - 2.5Y 8/1 white	6/N gray	fine	reduced	smoothed-polished internal /external surface	postfiring painting external surface <i>graffited</i> internal surface
MX3	Port	vessel	body	7.5YR 5/4 brownish	7.5YR 5/4 brownish	7.5YR 5/4 brownish	fine	oxidized	smoothed-polished internal /external surface	postfiring painting external surface <i>graffited</i> internal surface

Table 2. PIXE concentrations for major, minor, and trace elements (n=28)

Sample	Colour	MAJOR (wt%)											MINOR AND TRACES ( $\mu\text{g/g}$ )													
		C	O	Mg	Al	Si	K	Ca	Ti	Mn	Fe	Na	P	S	Cl	Sc	V	Cr	Ni	Cu	Zn	Rb	Sr	Zr	Ba	Pb
M1B	Black <sup>a</sup>	-	33.7	1.3	4.38	11.1	3.6	6.38	0.7	27.7	8.96	6593	1775	-	973	-	1102	-	-	569	1075	-	641	197	9691	-
M50B	Black <sup>a</sup>	-	38	1.7	4.58	17	5.8	7.97	0.9	12.7	9.83	5590	529	1041	994	-	826	-	-	261	381	-	1086	-	4764	-
M18B	Black <sup>a</sup>	-	35.8	1.1	5.55	13.6	4	6.09	0.5	21	9.41	14683	-	2213	6547	-	1370	-	-	202	204	147	592	-	4575	-
M24B	Black <sup>b</sup>	2.91	39.2	0.9	4.29	16.1	0.9	8.39	0.4	17.3	8.77	3026	2536	418	1787	-	-	-	-	231	227	-	770	-	-	-
M15B	Black <sup>b</sup>	1.58	32.4	0.6	3.93	12.9	1.4	0.05	0.3	16.4	29.1	4438	772	655	665	94	670	80	112	591	281	-	-	-	5232	-
M2Br	Burgundy <sup>a</sup>	-	41.1	1.3	9.24	18.8	10	2.79	1.6	0.24	13.4	6869	569	427	343	-	232	172	-	4943	734	694	296	380	-	92
M15Br	Burgundy <sup>a</sup>	-	38.2	1.2	4.5	14.5	5	4.02	0.6	0.14	30.4	11542	488	1967	617	-	-	78	-	182	160	-	350	-	-	-
M18Br	Burgundy <sup>a</sup>	-	36.7	0.9	4.41	13.6	7	3.3	0.8	0.2	27.7	36518	-	974	15690	-	-	149	-	694	579	-	209	-	-	-
M28DB	Dark Brown <sup>a</sup>	-	33.8	0.9	2.7	7.95	2.2	10.7	0.3	8.33	31.9	3101	2843	980	232	-	481	-	-	211	-	-	724	-	4545	-
M31LB	Light Brown <sup>a</sup>	-	39.3	2.7	8.37	15.5	9.3	4.68	1.6	3.04	14.5	5917	847	700	768	-	-	152	263	201	357	116	300	351	-	-
M38R	Reddish <sup>a</sup>	-	40.1	0.9	8.28	16.8	7.4	4.01	1.2	0.39	20.2	4503	402	500	2337	-	-	131	-	154	94	181	285	143	-	-
MXR	Reddish <sup>a</sup>	-	39.9	0.8	8.32	16.5	8	6.65	1.1	0.16	17.9	4640	1445	353	324	-	-	128	-	114	525	177	135	258	-	-
M7R	Reddish <sup>b</sup>	3.32	41	0.6	4.72	25.3	4.8	1.07	0.4	0.15	17.3	10246	1725	1102	384	-	-	82	152	-	312	-	-	-	-	-
M13W	White <sup>a</sup>	-	41.3	1.1	8.25	19.4	6.3	14.1	1	0.07	7.1	7222	1366	378	1771	-	-	152	-	1838	450	-	348	-	-	225
M28W	White <sup>a</sup>	-	38	0.8	5.87	14.1	5.3	25.5	0.9	1.03	7.75	3204	2804	1375	879	-	-	-	-	32	88	-	-	609	-	-
M47W	White <sup>a</sup>	-	39.1	1.6	7.29	14.6	2.6	26.3	0.9	0.22	6.47	3034	2313	465	1704	-	-	110	-	302	297	-	568	-	-	294
M57W	White <sup>a</sup>	-	38.8	2.2	6.38	14.2	2.4	25	1.1	1.34	6.35	8562	2830	2803	1518	-	-	179	-	496	966	208	1007	539	2505	543
M16W	White <sup>a</sup>	-	35.2	1.3	3.23	9.7	3.1	42.3	0.6	0.15	2.97	4155	2138	4309	2433	-	-	137	-	166	127	-	604	-	-	163
M45W	White <sup>a</sup>	-	39.2	2.5	6.86	14.8	2.7	26.9	0.9	0.16	3.62	14918	2297	849	3129	-	149	-	-	128	510	-	476	-	-	133
M24W	White <sup>b</sup>	6.32	43.4	1	7.94	20.4	1.8	14.7	0.4	0.16	2.81	4446	3374	723	2260	1081	-	34	-	143	-	102	-	-	-	-
M52W	White <sup>b</sup>	1.65	41.2	1.5	10	21.2	1.7	15.8	0.6	0.09	3.47	18503	6852	126	1099	701	-	376	-	70	653	-	-	-	-	-
M16O	Ocher <sup>a</sup>	-	42.9	1	7.13	23	6.9	8.47	1	0.18	8.21	7825	2115	782	443	-	-	107	50	215	248	351	395	-	-	41
M24O	Ocher <sup>b</sup>	6.27	45.4	0.9	5.81	26.1	3.2	7.11	0.4	0.04	3.62	5596	3711	1013	605	-	-	59	45	26	157	111	223	242	-	-
M9P	Paste <sup>a</sup>	-	43.6	1.7	8.35	23.4	7.2	3.54	1.3	0.3	9.27	7937	1062	410	2389	-	-	95	47	91	255	202	362	596	-	-
M49P	Paste <sup>a</sup>	-	42.8	1.7	5.95	23	4.2	13.2	0.7	0.13	6.77	12057	680	690	622	-	121	-	86	-	171	134	460	-	-	-
MX3P	Paste <sup>a</sup>	-	43.9	0.9	9.36	24.1	9.3	3.6	1.5	0.15	5.9	8126	1421	590	1346	-	-	205	147	-	420	244	403	174	-	269
M7P	Paste <sup>b</sup>	2.42	41.4	1.4	11	24.6	7.6	3.11	0.8	0.12	5.79	15400	1178	1251	375	-	-	158	197	50	275	-	-	-	-	-
M15P	Paste <sup>b</sup>	1.5	43.3	0.9	11.2	23.3	4.9	1.21	0.8	0.1	11.1	12127	784	1385	1381	78	178	105	170	78	158	-	-	-	-	-

Table 3. Element concentration and standard deviations (mean +SD) for the paintings compositional groups.

Element	Group 1 (n= 5)	Group 2 (n=7)	Group 3 (n=9)
C (%)	2.73 ±0.39	3.06±1.52	2.70±0.44
O (%)	36.10±2.47	39.25±2.55	40.62±2.31
Na	6598.6±4779	8117.42±6237	11753.44±9897
Mg (%)	1.15±0.33	1.55±0.61	1.07±0.36
Al (%)	4.3±1.02	6.79±2.06	7.57±2.41
Si (%)	13.15±3.71	15.57±3.97	19.71±4.64
P	1841.81±909	3229.71±1652	1036.57±465.22
S	984.29±765	1521.42±1504	841.56±535
Cl	2106.6±2545	1860.28±793	2645±4963
K (%)	3.27±1.85	2.80±1.20	7,36±1.71
Ca (%)	7.90±1.85	25.19±9.08	3.57±1.46
Sc	324.84±54.11	480.60±319	231.62±76.50
Ti (%)	0.53±0.24	0.77±0.23	1.03±0.41
V	845.18±397	384.29±153	376.02±122.33
Cr	127.80±41.18	154.34±107.46	133.11±42.84
Mn (%)	17.39±7.46	0.45±0.51	0.21±0.09
Fe (%)	13.77±10.13	4.77±2.01	16.43±8.83
Ni	94.29±30.65	111.28±34.47	121.89±43.43
Cu	294.8±154	191±159.25	716.89±1596.83
Zn	423.36±370	423.78±311	372.67±208.72
Rb	199.91±60.93	182.30±50.49	232.45±177.16
Sr	762.6±193.66	580.49±196	309.86±89.28
Zr	324.56±86.41	418.51±131.35	298.45±135.16
Ba	5637.50±2267	4351.50±993	4935.55±607.56
Pb	174.65±120	235.26±148.13	198.06±67.89





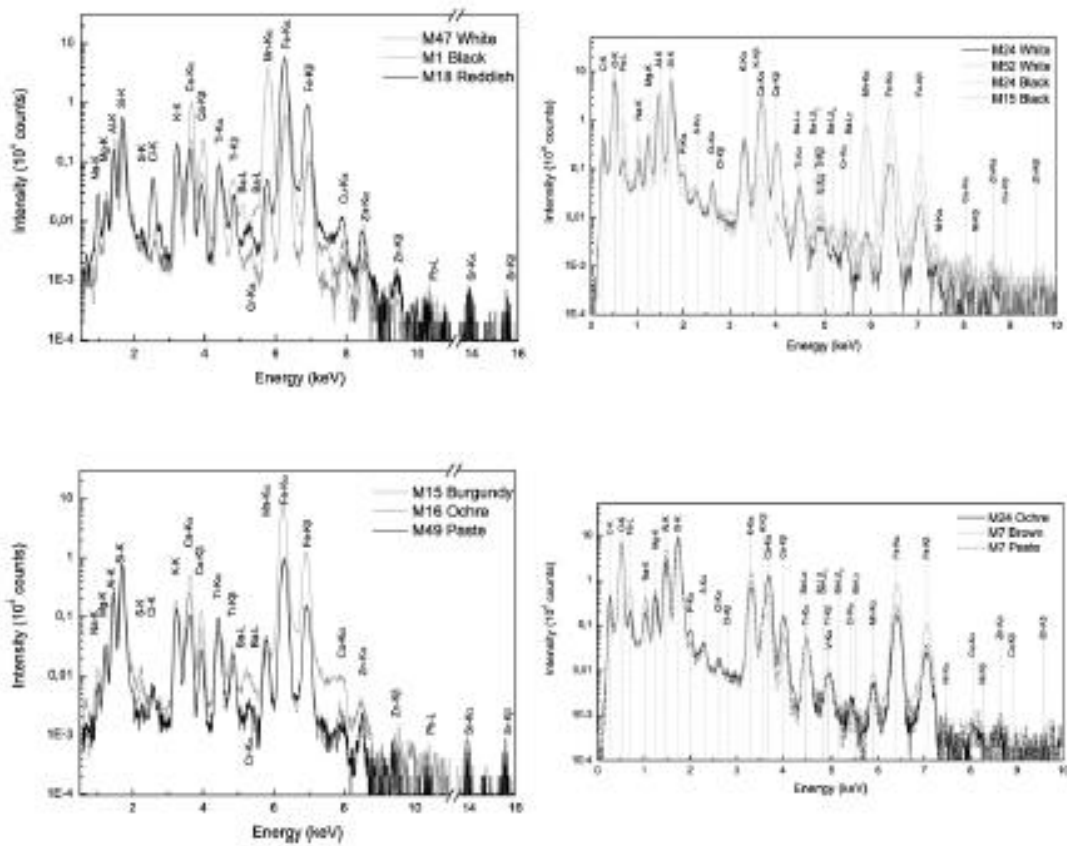


Figure 2. PIXE spectra for 2 MeV for some of the white, black, reddish, ochre and brown paints. Measurements acquired in the NEC 3MV, UFRGS (left), and at Tandem 1.7MeV, CAB (right). Elements determined are shown in the figures.

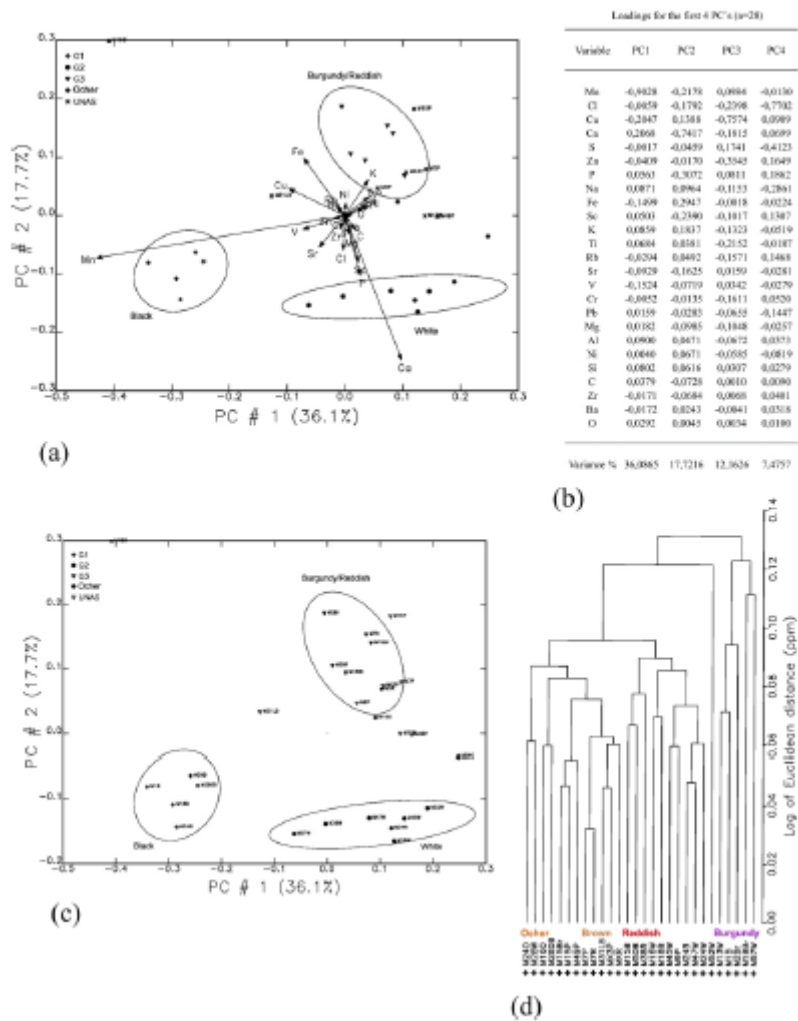


Figure 3. (a) PCA of major, minor and trace elements showing the discriminated colour groups (G1:black, G2:white, and G3:burgundy/reddish). UNAS: unassigned samples. Projected elements are also shown (ellipses represent 95% confidence); (b) Loadings for the first 4 PC's (n=28); (c) PC1 and PC2 showing Groups 1, 2 and 3, defined by Mahalanobis distances (ellipses represent 95% confidence); (d) Cluster analysis of minor and trace elements, showing the discrimination of the red iron oxides based pigments.

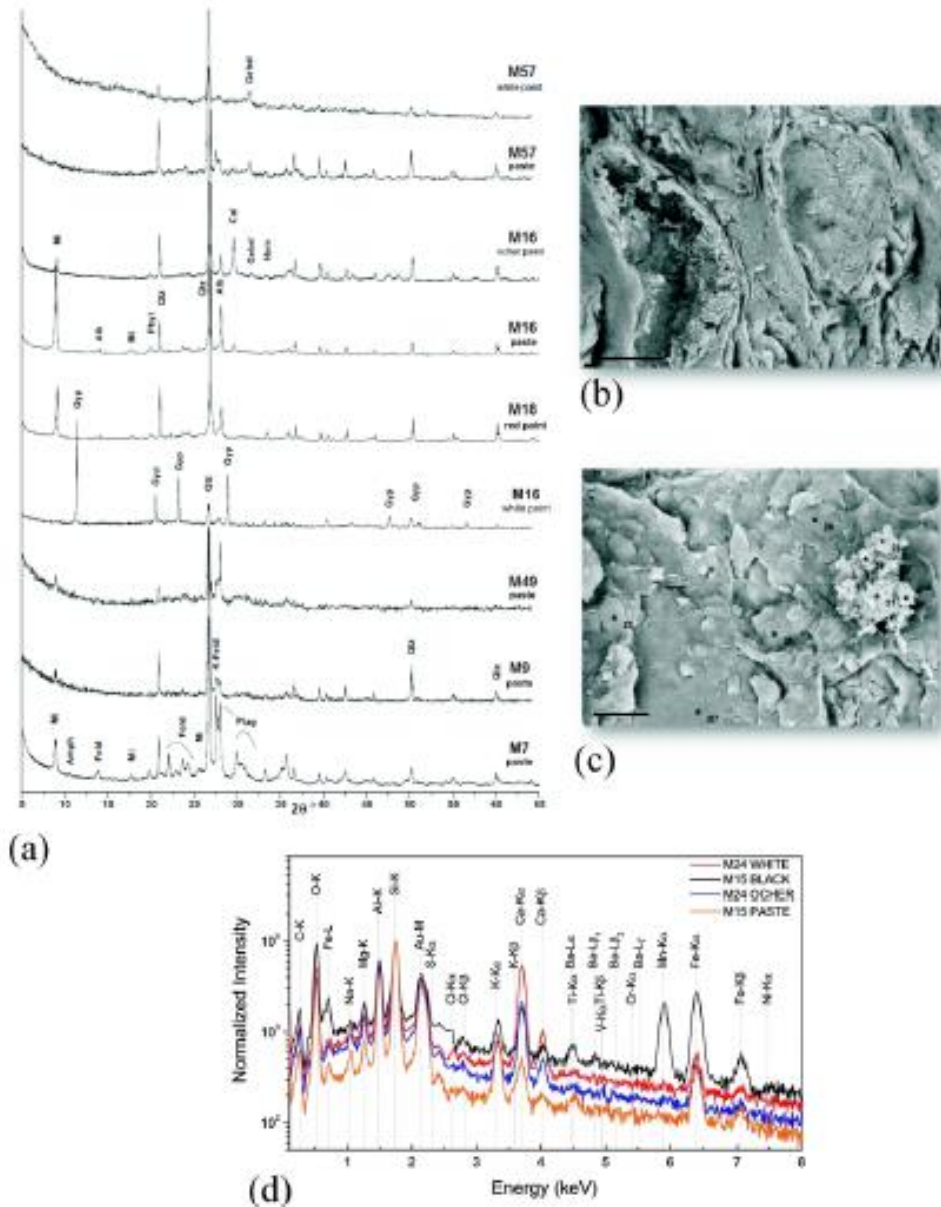


Figure 4. (a) XRD spectra for white prefiring slip, ocher and reddish postfiring paints. Also, some paste samples are shown; (b) SEM secondary electron images for M15 sample showing (a) vitrified textures; (c) neoformation mineral phases; (d) EPMA spectra for M15 (black), M24 (white), M24 (ocher), and M15 (paste).

A